Frequency robust control in stand-alone microgrids with PV sources : design and sensitivity analysis

Quang Linh Lam, Antoneta Iuliana Bratcu, Delphine Riu

Frequency robust control in stand-alone microgrids with PV sources : design and sensitivity analysis

Quang Linh LAM[1,2], Antoneta Iuliana BRATCU[2], and Delphine RIU[1]
[1]G2Elab, Grenoble Electrical Engineering Laboratory
UMR 5269 CNRS – Grenoble INP – Université Grenoble Alpes
F-38031 Grenoble Cedex 1, France
(E-mail : Quang-Linh.Lam, Delphine.Riu@g2elab.grenoble-inp.fr)
[2]GIPSA-lab, Grenoble Department of Control Systems
UMR 5216 CNRS – Grenoble INP – Université Grenoble Alpes
F-38402 Saint Martin d'Hères Cedex, France
(E-mail : Antoneta.Bratcu@gipsa-lab.grenoble-inp.fr)

ABSTRACT – In this paper, a robust $\mathcal{H}_\infty$ control strategy for frequency regulation is proposed in isolated microgrids (MGs) composed of diesel engine generators, photovoltaic (PV) sources, and storage units. First, the linear matrix inequalities (LMI) method is adopted to design a multi-variable $\mathcal{H}_\infty$ controller which ensures given specifications. In a second step, uncertainties in the storage device state of charge (SoC) are considered and a sensitivity analysis is carried out in order to determine the maximum variation range of SoC for which the dynamic performances are respected. The controller's robustness and performance in the presence of various load disturbances, PV output power variations, and the SoC uncertainty are validated through a series of nonlinear time-domain simulations performed with MATLAB®/Simulink®.

Keywords – Microgrids, frequency control, robust control, multi-variable control, uncertainty, sensitivity analysis.

1. INTRODUCTION

MGs emerge as a major, cost-effective solution for the integration of Distributed Energy Resources (DERs) into power systems, as they offer enhanced global reliability, higher energy efficiency, and various environmental and economic advantages [1]. MG stability and control issues are however among the main challenges, especially during islanded mode due to low inertia, uncertainties, and intermittent nature of DERs [2]. Maintaining frequency and voltage deviations within their predefined range is critical in autonomous operation mode. High-speed storage systems – e.g., lithium-ion batteries, flywheels or supercapacitors – have thus become necessary, leading to new grid configurations, for which more complex robust control structures are needed for dealing with multiple constraints such as unexpected disturbances and model uncertainties.

$\mathcal{H}_\infty$ control theory applied to frequency regulation has attracted the attention of many researchers for several reasons. First, many control objectives such as disturbance attenuation, robust stabilization of uncertain systems or shaping of the open-loop response can be handled by $\mathcal{H}_\infty$– and μ–synthesis techniques [3]. Then, the solution found is optimal with respect to a defined criterion, which means that if no solution to the control objectives is found, then no solution exists. Finally, sensitivity and robustness analysis to model uncertainties can possibly be associated with $\mathcal{H}_\infty$ and μ–synthesis controls.

Some studies on robust control techniques for various MGs have already been conducted. In [4], $\mathcal{H}_\infty$-based droop frequency control is given. System trade-offs are optimized ; however, robustness to model uncertainties is not considered. $\mathcal{H}_\infty$ control with loop shaping and $\mathcal{H}_\infty$-based droop control for improving frequency deviation are presented in [5], but only controller sensitivity to parameter uncertainties is analyzed. Parameter uncertainties are considered in designing $\mathcal{H}_\infty$ and μ–synthesis controls for the voltage direct single-loop in [6]. Conventional $\mathcal{H}_\infty$-based and μ minimization approaches for the direct single-loop current control scheme are also adopted in [7]. Multi-variable $\mathcal{H}_\infty$ control is utilized in [8] to design robust controllers to system nonlinearities and load interactions. [9] introduces a μ–synthesis robust control method for a grid-tied PV generation system taking parameter variations into account. In [10], $\mathcal{H}_\infty$ and μ–synthesis robust controls under parametric uncertainties for improving secondary frequency control performance are applied.

Our work focuses on the frequency stability problem of MGs with high penetration of renewable energy. Frequency deviation can be considerably reduced by using relatively small storage units, provided that saturation conditions are avoided, by dynamically coordinating storage with other generation sources [11]. This paper proposes a multi-variable $\mathcal{H}_\infty$ robust controller for primary frequency regulation that copes with load transients, PV output power variations, and model uncertainties. A sensitivity analysis is then conducted according to system parameters.

The remainder of this paper is structured as follows. Section 2 introduces the studied MG setup. Section 3 is devoted to the proposed control methodology. Dynamic specifications are presented in Section 4. Section 5 provides system modeling for $\mathcal{H}_\infty$ control. The detailed process of designing the $\mathcal{H}_\infty$ controller, along with some nonlinear time-domain simulations with respect to the rated operating point, are described in Section 6. Section 7 details the sensitivity analysis of robust performance of the $\mathcal{H}_\infty$ controller when the supercapacitor voltage v_{sc} – which is an image of its SoC_{sc} – is considered a time-variant parameter ; the controller robustness is then demonstrated through a series of nonlinear time-domain simulations. Some concluding remarks and future work are drawn in Section 8.

2. MICROGRID STRUCTURE

This paper focuses on an islanded MG constituted by a diesel engine generator, a PV source and a supercapacitor-based energy storage unit. The studied MG setup is illustrated in Fig. 1 [12], where power sources are connected in parallel to a point of common coupling (PCC) and feed a common load. The PV panel bank is connected to the PCC through a chopper – inverter without reversibility allowing only unidirectional power flow, whereas the supercapacitor-based storage device is connected

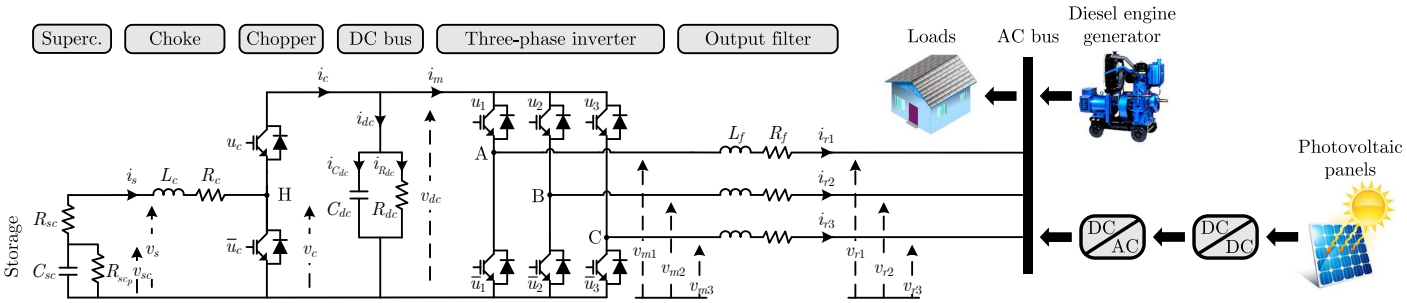

Fig. 1. Studied MG setup [12].

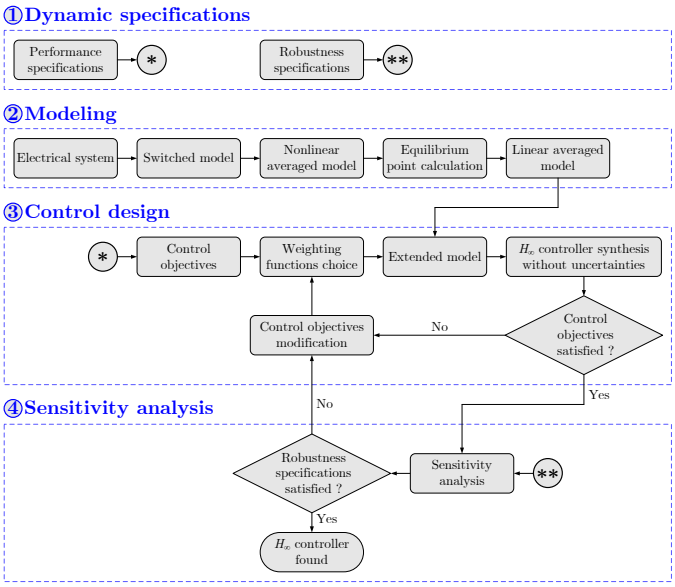

Fig. 2. Proposed control methodology.

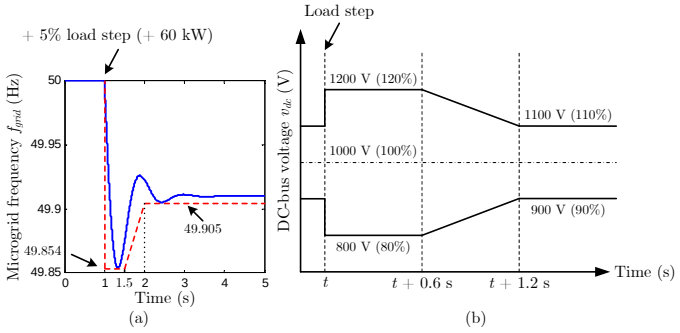

Fig. 3. (a) MG frequency time-domain performance specifications consequent to a load step of + 5% of the rated load power (+ 60 kW) [12], [14]. (b) DC-bus voltage time-domain performance specifications consequent to a load step.

to the PCC and controlled by means of a reversible chopper – inverter, which allows charging or discharging.

3. PROPOSED CONTROL METHODOLOGY

In order to reduce the time spent for control design, a generalized methodology taking the controller robustness into account is used. Then, it allows minimizing the number of back and forth steps in the design process. This methodology is resumed in Fig. 2 and can be divided into four steps which are detailed below :

- First, performances and robustness levels are specified by the designer according to standards ;
- Afterwards, dynamical equations and equivalent averaged models of power-electronic converters are used to describe the behavior of an electrical system. By linearizing these equations for a given equilibrium state a linear state-space model can be obtained ;
- In order to respect performances, a control architecture is then designed for nominal values using $\mathcal{H}_\infty$ control. Control objectives are introduced using weighting functions over particular closed-loop transfer functions [13]. An extended model including these weighting functions is then obtained. An optimal controller can now be computed using control tools in the MATLAB® software environment. A multi-variable $\mathcal{H}_\infty$ controller is obtained until all desired control objectives are satisfied. For control validation, closed-loop time-domain simulations using the averaged models are convenient ;
- Finally, a sensitivity analysis is carried out to test the validation for desired $\mathcal{H}_\infty$ controller robustness. If this is not satisfied, the control objectives must be modified and the step 3 is re-conducted.

4. DYNAMIC SPECIFICATIONS

In the literature, coordinated strategy of the energy storage system and the diesel engine generator in primary frequency control has been proposed in order to improve dynamic performances (lower overshoot, faster response time, smaller steady-state error) of the frequency f_{grid} in case of load power variations. Control design is performed for given frequency performance requirements shown in Fig. 3(a) [12], [14]. Another reasonable performance specifications on the DC-bus voltage v_{dc} are given in Fig. 3(b). Robustness specifications will be introduced later.

5. SYSTEM MODELING FOR $\mathcal{H}_\infty$ CONTROL

A cascaded two-level control structure (Fig. 4) – where classical PI-based current tracking controllers are placed on the low control level and receive references from an $\mathcal{H}_\infty$-control-based upper level – is developed to ensure the previous dynamic specifications. The current control level is detailed in [12]. System modeling for $\mathcal{H}_\infty$ control loop is given in this Section.

A per-unitized linear averaged model of the storage system together with its power-electronic converters, as well as a linear state-space representation of the considered MG around a steady-state equilibrium point, for $\mathcal{H}_\infty$ control loop design, are presented. In this paper, the supercapacitor voltage v_{sc} is regarded as a time-invariant parameter (i.e., $v_{sc} = v_{sc_e}$ or $\Delta v_{sc} = 0$) in $\mathcal{H}_\infty$ controller synthesis. Note that the supercapacitor voltage depends in reality on the supercapacitor current ; a sensitivity analysis considering variation of this parameter is presented in Section 7. Hence, the resulting small-signal state-space model

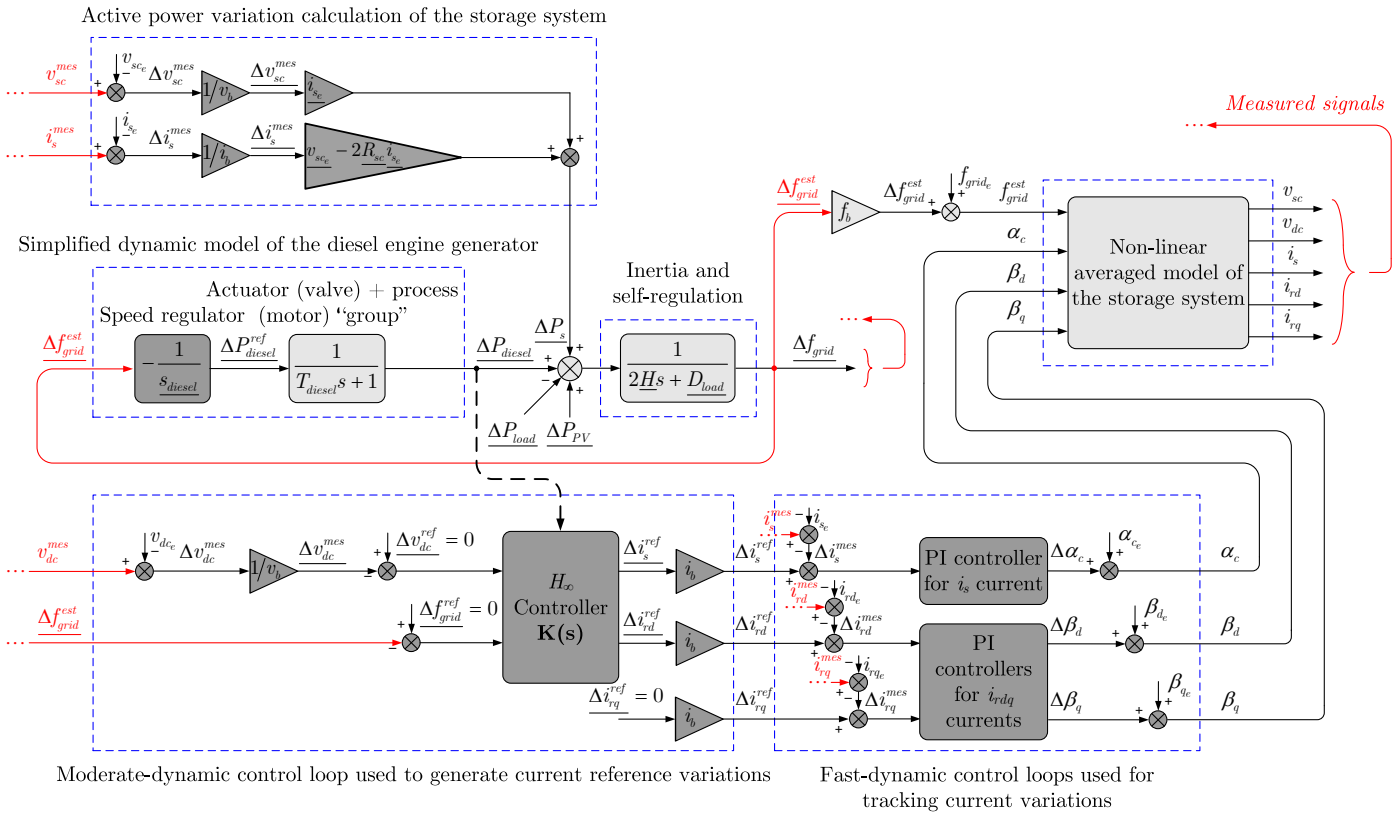

Fig. 4. Block diagram of the proposed global control structure.

is given as follows

$$\begin{cases} \underline{\mathbf{\Delta \dot{x}}} = \mathbf{A}\underline{\mathbf{\Delta x}} + \mathbf{B_1}\underline{\mathbf{\Delta u}} + \mathbf{B_2}\underline{\mathbf{\Delta w}} \\ \underline{\mathbf{\Delta y}} = \mathbf{C}\underline{\mathbf{\Delta x}} + \mathbf{D_1}\underline{\mathbf{\Delta u}} + \mathbf{D_2}\underline{\mathbf{\Delta w}} \end{cases}, \tag{1}$$

where the underline denotes per-unitized values. The state vector $\underline{\mathbf{\Delta x}} = \left[\begin{array}{ccc} \underline{\Delta v_{dc}} & \underline{\Delta P_{diesel}} & \underline{\Delta f_{grid}} \end{array}\right]^T$ consists of the DC-bus voltage variation, the diesel engine generator power variation, and the frequency variation. $\underline{\mathbf{\Delta u}} = \left[\begin{array}{cc} \underline{\Delta i_s^{ref}} & \underline{\Delta i_{rd}^{ref}} \end{array}\right]^T$ is the control input vector composed of the storage device current reference variation and the inverter output current reference variation in d–axis. $\underline{\mathbf{\Delta w}} = \underline{\Delta P_{load}} - \underline{\Delta P_{PV}}$ is the load and PV output power variation, which represents the disturbance input. $\underline{\mathbf{\Delta y}} = \left[\begin{array}{cc} \underline{\Delta v_{dc}} & \underline{\Delta f_{grid}} \end{array}\right]^T$ is the measured output vector. Matrices in (1) are given by

$$\mathbf{A} = \begin{bmatrix} -\frac{\omega_b}{\underline{R_{dc}}\underline{C_{dc}}} & 0 & 0 \\ 0 & -\frac{1}{\underline{T_{diesel}}} & -\frac{1}{\underline{T_{diesel}}\underline{s_{diesel}}} \\ 0 & \frac{1}{2\underline{H}} & -\frac{\underline{D_{load}}}{2\underline{H}} \end{bmatrix},$$

$$\mathbf{B_1} = \begin{bmatrix} \frac{\omega_b}{\underline{C_{dc}}}\alpha_{c_e} & -\frac{\omega_b}{\underline{C_{dc}}}\beta_{d_e} \\ 0 & 0 \\ \frac{1}{2\underline{H}}\left(\underline{v_{sc_e}} - 2\underline{R_{sc}}\underline{i_{s_e}}\right) & 0 \end{bmatrix}, \mathbf{B_2} = \begin{bmatrix} 0 \\ 0 \\ -\frac{1}{2\underline{H}} \end{bmatrix},$$

$$\mathbf{C} = \begin{bmatrix} 1 & 0 & 0 \\ 0 & 0 & 1 \end{bmatrix}, \mathbf{D_1} = \begin{bmatrix} 0 & 0 \\ 0 & 0 \end{bmatrix}, \mathbf{D_2} = \begin{bmatrix} 0 \\ 0 \end{bmatrix},$$

where $\underline{s_{diesel}}$ is the droop value, T_{diesel} denotes the time constant of the diesel engine generator. α_c is the average value of the chopper duty ratio, β_d is the average value of the inverter switching function in d–axis. $\underline{H}$ is the MG equivalent inertia constant. $\underline{D_{load}}$ is the load damping constant. Subscript e indicates the steady-state equilibrium point. Steady-state real-unit values are given in Table 1. Note that the v_{sc_e} value chosen for $\mathcal{H}_\infty$ control design corresponds here to the range middle between the minimum and maximum supercapacitor voltages. In this case, $v_{sc_e} = 585$ V, where 390 V ($SoC_{sc} = 25\%$) is taken as the minimum and 780 V ($SoC_{sc} = 100\%$) is the maximum values of v_{sc}.

Table 1. Steady-state real-unit values of the linearized system

Variable	v_{sc_e}	v_{dc_e}	v_{rd_e}	v_{rq_e}	i_{s_e}
Value	585 V	1000 V	400 V	0 V	−2.5 A
Variable	i_{rd_e}	i_{rq_e}	α_{c_e}	β_{d_e}	β_{q_e}
Value	−18.7 A	0 A	0.585	0.4	−0.0027
Variable	P_{diesel_e}	P_{PV_e}	P_{load_e}	f_{grid_e}	ω_{grid_e}
Value	1.0015 MW	0.2 MW	1.2 MW	50 Hz	100π rad/s

6. $\mathcal{H}_\infty$ CONTROL DESIGN

6.1. *Control design*

The design of a multi-variable $\mathcal{H}_\infty$ controller for the system (1) is cast into the formalism in Fig. 5, where weighting functions $W_{perf}(s)$ are chosen to guarantee the performance objectives. The practical implementation constraints imposed to the control inputs are dealt with by choosing weighting functions $W_u(s)$.

The linear time-invariant (LTI) weighting functions, used for a S/KS mixed-sensitivity optimization process to reject distur-

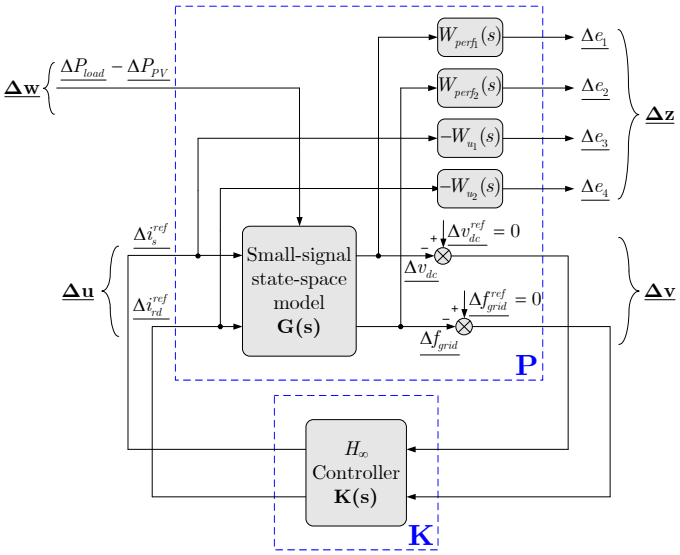

Fig. 5. Control configuration in the so-called $\mathbf{P}-\mathbf{K}$ form, where $\mathbf{P}$ denotes the plant together with the weighting functions and $\mathbf{K}$ denotes the $\mathcal{H}_\infty$ controller.

Table 2. Weighting function parameters $W_{perf}\,(s)$

	$W_{perf_1}\,(s)$ for $\underline{\Delta v_{dc}}$	$W_{perf_2}\,(s)$ for $\underline{\Delta f_{grid}}$
M_s	$\frac{0.02\underline{v_{dc_e}}}{0.05\underline{P_{load_e}}} = 1.667$	$\frac{(50.12-50)/f_b}{0.05\underline{P_{load_e}}} = 0.08$
A_ε	$\frac{0.01\underline{v_{dc_e}}}{0.05\underline{P_{load_e}}} = 0.833$	$\frac{(50.06-50)/f_b}{0.05\underline{P_{load_e}}} = 0.04$
ω_b	$1\Big/\left(40T_{0_{rdq}}\right) = 2.61$ rad/s (response time $t_{r_1} \approx 1.2$ s)	$1\Big/\left(20T_{0_{rdq}}\right) = 5.22$ rad/s (response time $t_{r_2} \approx 0.6$ s)

bance due to the load power variation, are written as follows

$$\begin{cases} \frac{1}{W_{perf}(s)} = \frac{s+\omega_b A_\varepsilon}{s/M_s+\omega_b},\ \frac{1}{W_{u_2}(s)} = \frac{A_{u_2}s+\omega_{bc_2}}{s+\omega_{bc_2}/M_{u_2}} \\ \frac{1}{W_{u_1}(s)} = A_{u_1}\frac{\left(\frac{M_{u_1}}{\omega_{bc_{11}}}s+1\right)\left(\frac{A_{u_1}}{\omega_{bc_{12}}}s+1\right)}{\left(\frac{A_{u_1}}{\omega_{bc_{11}}}s+1\right)\left(\frac{M_{u_1}}{\omega_{bc_{12}}}s+1\right)},\ \frac{\omega_{bc_{11}}}{A_{u_1}} < \frac{\omega_{bc_{12}}}{M_{u_1}} \end{cases} . \quad (2)$$

The DC-bus voltage variation $\underline{\Delta v_{dc}}$ and the frequency variation $\underline{\Delta f_{grid}}$ are bounded by first-order weighting functions $W_{perf}\,(s)$. The function $1/W_{perf}\,(s)$ can be representative of time-domain response specifications, where the high-frequency gain M_s has an influence on the system overshoot, the cut-off frequency ω_b tunes the desired response time and the low-frequency gain A_ε allows limiting the steady-state error. That makes equivalences between desired time-domain performances and frequency-domain specifications (Fig. 6). The active power injection or absorption of the storage system is controlled via i_s. Thus, the storage device current reference variation $\underline{\Delta i_s^{ref}}$ is bounded by a band-pass weighting function $W_{u_1}\,(s)$. The DC-bus voltage is regulated via i_{rd}. The inverter output current reference variation in d–axis $\underline{\Delta i_{rd}^{ref}}$ is bounded by the first-order weighting function $W_{u_2}\,(s)$. Frequency-domain specifications on these current reference variations are presented in Fig. 7. The parameters of the weighting functions are given in Table 2 and Table 3, where $1/T_{0_{rdq}}$ is the Δi_{rd} inner closed-loop bandwidth.

The LMI algorithm under the MATLAB® software environment yields a solution after one iteration for a multi-variable

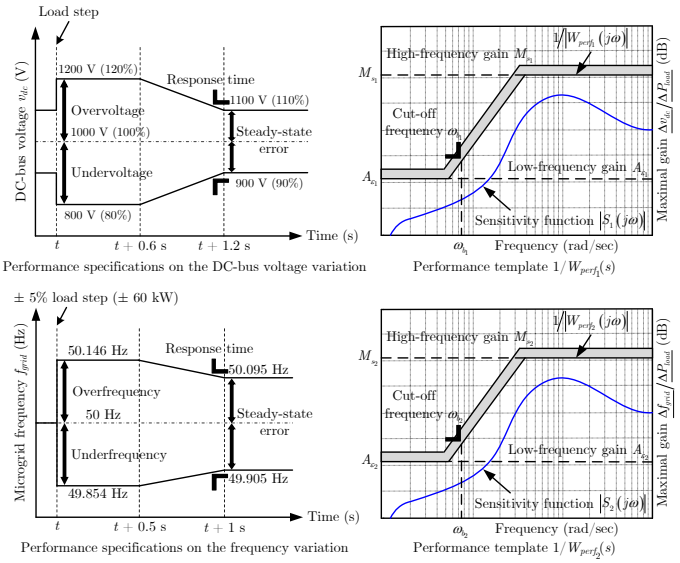

Fig. 6. Translation of temporal norms into frequency-domain specifications.

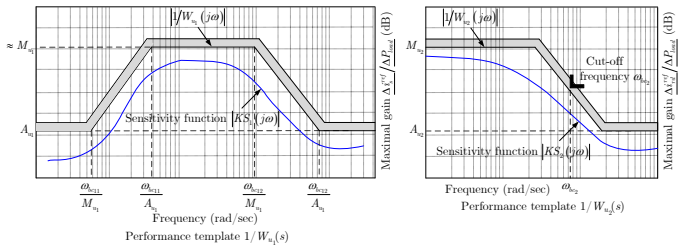

Fig. 7. Frequency-domain specifications on the energy storage device current reference variation $\underline{\Delta i_s^{ref}}$ and the inverter output current reference variation in d–axis $\underline{\Delta i_{rd}^{ref}}$.

full-order $\mathcal{H}_\infty$ controller which has 8 states with a conditioning value of $\gamma = 1301.27$ and an $\mathcal{H}_\infty$ norm = 3.48.

For the studied system shown in Fig. 5, sensitivity functions $S_1\,(s)$, $S_2\,(s)$ and complementary sensitivity functions $KS_1\,(s)$, $KS_2\,(s)$ are defined by

$$\begin{cases} S_1\,(s) = \frac{\Delta v_{dc}(s)}{\Delta P_{load}(s)},\ S_2\,(s) = \frac{\Delta f_{grid}(s)}{\Delta P_{load}(s)} \\ KS_1\,(s) = \frac{\Delta i_s^{ref}(s)}{\Delta P_{load}(s)},\ KS_2\,(s) = \frac{\Delta i_{rd}^{ref}(s)}{\Delta P_{load}(s)} \end{cases} . \quad (3)$$

The singular value plots of the MIMO sensitivity functions $S(s)$, complementary sensitivity functions $KS(s)$, and corresponding templates are shown in Fig. 8. Results show how the shaping of $\mathcal{H}_\infty$ performance is straightforward for the full-order $\mathcal{H}_\infty$ controller using the template weighting functions. One can see that control performance weights imposed are well-respected since the sensitivity functions are placed below the corresponding templates regardless of the frequency value.

6.2. *Time-domain simulation results*

In order to validate the effectiveness of the proposed control approach, MATLAB®/Simulink® time-domain simulations are performed on the nonlinear averaged model. The impact of PV output active power variations on the microgrid frequency is analyzed with or without secondary control ($K_i \neq 0$ or $K_i = 0$), where K_i denotes the inverse of the response time

Table 3. Weighting function parameters $W_u(s)$

	$W_{u_1}(s)$ for $\underline{\Delta i_s^{ref}}$	$W_{u_2}(s)$ for $\underline{\Delta i_{rd}^{ref}}$
M_u	$\frac{\underline{i_{s_{max}}} - \underline{i_{s_e}}}{0.05\underline{P_{load_e}}} = 9.62$	$\frac{\underline{i_{rd_{max}}} - \underline{i_{rd_e}}}{0.05\underline{P_{load_e}}} = 8.46$
A_u	$0.1M_u = 0.962$	$0.1M_u = 0.846$
ω_{bc}	$\frac{\omega_{bc_{11}}}{A_{u_1}} = \omega_p = 3.04$ rad/s ($\omega_{bc_{11}} = 2.93$ rad/s) $\frac{\omega_{bc_{12}}}{M_{u_1}} = 60$ rad/s ($\omega_{bc_{12}} = 577.2$ rad/s)	$1/(100T_{s_i}) = 40$ rad/s, where $T_{s_i} = 1/f_{s_i}$, f_{s_i} is the inverter switching frequency

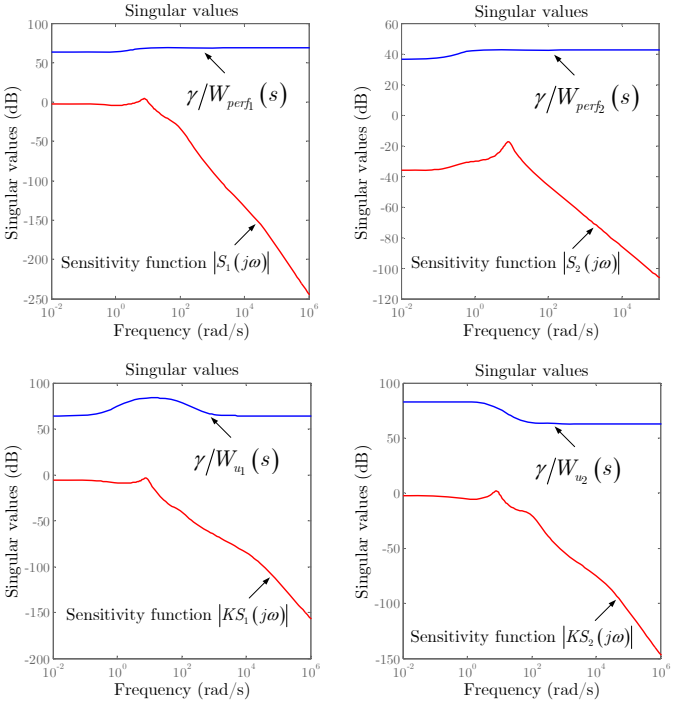

Fig. 8. Singular value plots for the sensitivity functions $S_1(s)$, $S_2(s)$; complementary sensitivity functions $KS_1(s)$, $KS_2(s)$; and corresponding templates.

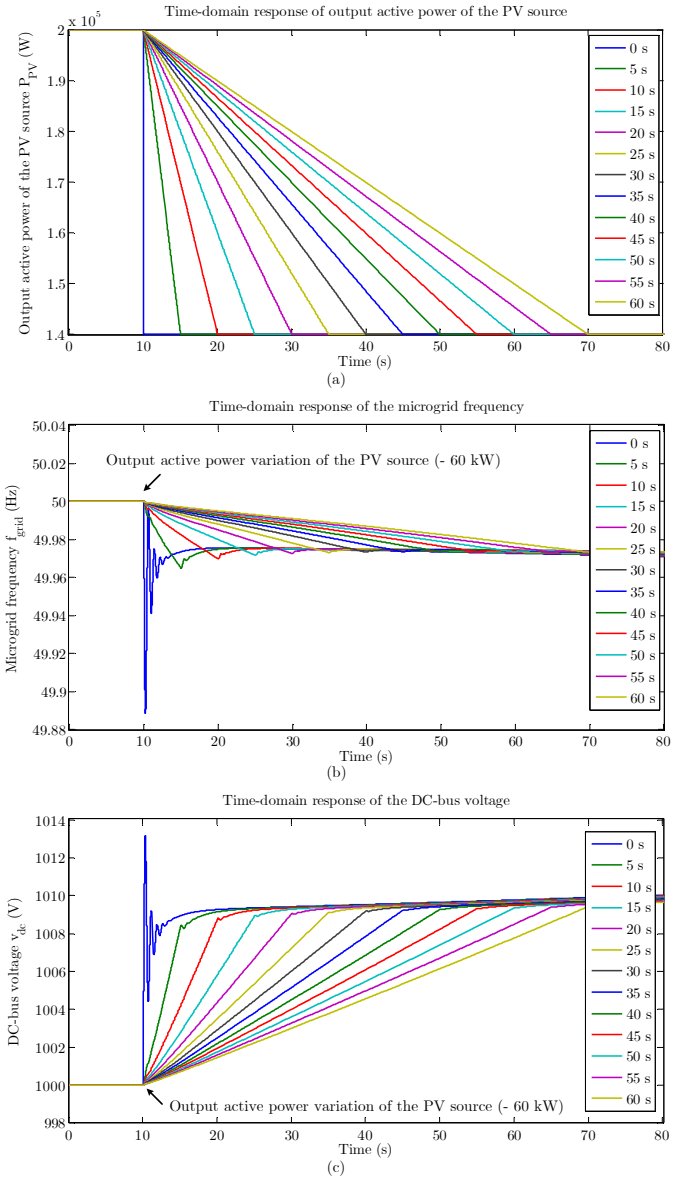

Fig. 9. (a) Time-domain responses of PV output active power (b) MG frequency time-domain responses f_{grid} and (c) DC-bus voltage time-domain responses v_{dc} under PV output active power disturbances of $-$ 60 kW with respect to the rated operating point.

of secondary control of the diesel engine generator. PV output active power variations modeled with different ramp signals are applied as disturbances. The PV output active power decreases by 60 kW from $P_{PV_e} = 200$ kW at $t = 10$ s to $P_{PV} = 140$ kW with different time durations Δt such as 0 s (step signal), 5 s, 10 s, ..., 60 s as shown in Fig. 9(a). The supercapacitor voltage v_{sc}, initially considered a time-invariant parameter in $\mathcal{H}_\infty$ controller synthesis, is regarded now as a time-variant one, i.e., $\Delta v_{sc} \neq 0$ (its dynamic equation, i.e., $\underline{\Delta \dot{v}_{sc}} = f\left(\underline{\Delta v_{sc}}, \underline{\Delta i_s}\right)$ being taken into account in the simulation model).

From Fig. 9(b) and Fig. 10(a) it can be observed that the MG frequency desired time-domain performances are successfully achieved with respect to choice of the weighting function $W_{perf_2}(s)$. Compared with the case in which only the diesel engine generator participates in primary frequency control, storage device participation has considerably improved the dynamic performances (i.e., lower overshoot, faster response time, smaller steady-state error) of the frequency. The system is also always stable. Secondary control participation of the diesel engine generator brings the frequency back to its nominal value of 50 Hz as shown in Fig. 10(a). Fig. 9(c) and Fig. 10(b) show that the DC-bus voltage desired time-domain performances corresponding to tuning of the weighting function $W_{perf_1}(s)$ are satisfied. Hence, the synthesized $\mathcal{H}_\infty$ controller guarantees the desired performance specifications.

7. SENSITIVITY ANALYSIS

In this Section, the sensitivity analysis of robust performance of the $\mathcal{H}_\infty$ controller is considered to answer the question whether the closed-loop system remains robust or not (from a performance point of view) to a given parametric uncertainty level in the steady-state value of the supercapacitor voltage v_{sc_e} around its design value, 585 V.

SoC_{sc} estimation is very important in determining the best operating strategy of the energy storage system. SoC_{sc} is approximated as the ratio between stored energy W_{sc}^* (Fig. 11) and

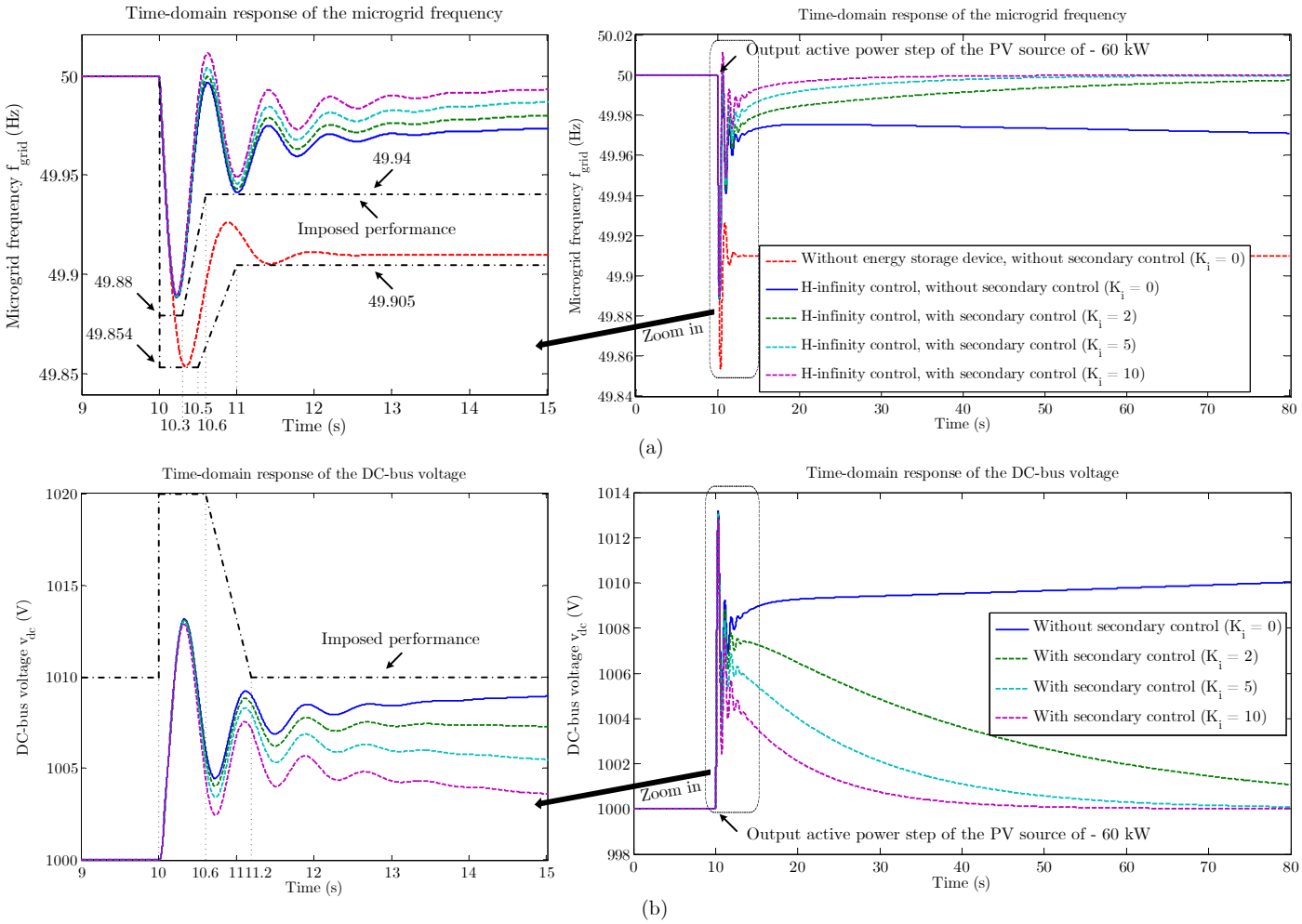

Fig. 10. (a) MG frequency time-domain responses f_{grid} and (b) DC-bus voltage time-domain responses v_{dc} under a PV output active power step disturbance of $-$ 60 kW with respect to the rated operating point.

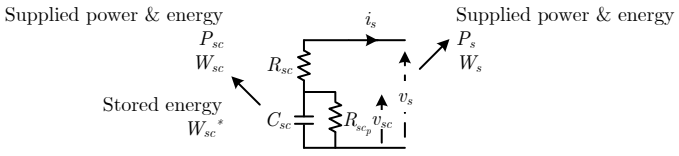

Fig. 11. Supercapacitor electrical scheme.

maximum storable energy $W^*_{sc_{max}}$ as follows (with the internal resistances R_{sc} and R_{sc_p} being neglected)

$$SoC_{sc} = \frac{W^*_{sc}}{W^*_{sc_{max}}} = \frac{\frac{1}{2}C_{sc}v^2_{sc}}{\frac{1}{2}C_{sc}v^2_{sc_{max}}} = \left(\frac{v_{sc}}{v_{sc_{max}}}\right)^2, \quad (4)$$

where $v_{sc_{max}} = 780$ V is the maximum possible supercapacitor voltage. In practice, SoC_{sc} is maintained within the admissible range of $[25, 100]$ % to ensure reliable, efficient, and safe operation of the supercapacitor and prolong its lifespan. The limited variation range, corroborated with (4), indicates that the v_{sc} value must be controlled between 390 V and 780 V.

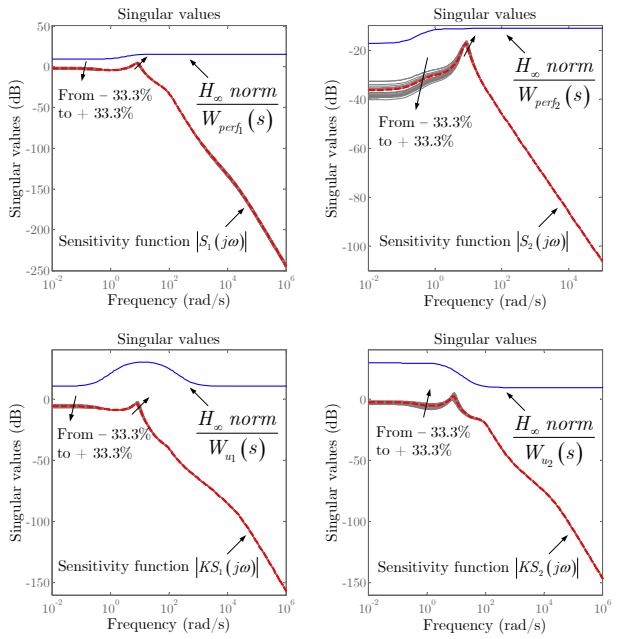

Fig. 12. Singular value plots of the sampled uncertain sensitivity functions $S_1(s)$, $S_2(s)$; complementary sensitivity functions $KS_1(s)$, $KS_2(s)$ obtained with 33.3% uncertainty in v_{sc_e}; and corresponding templates.

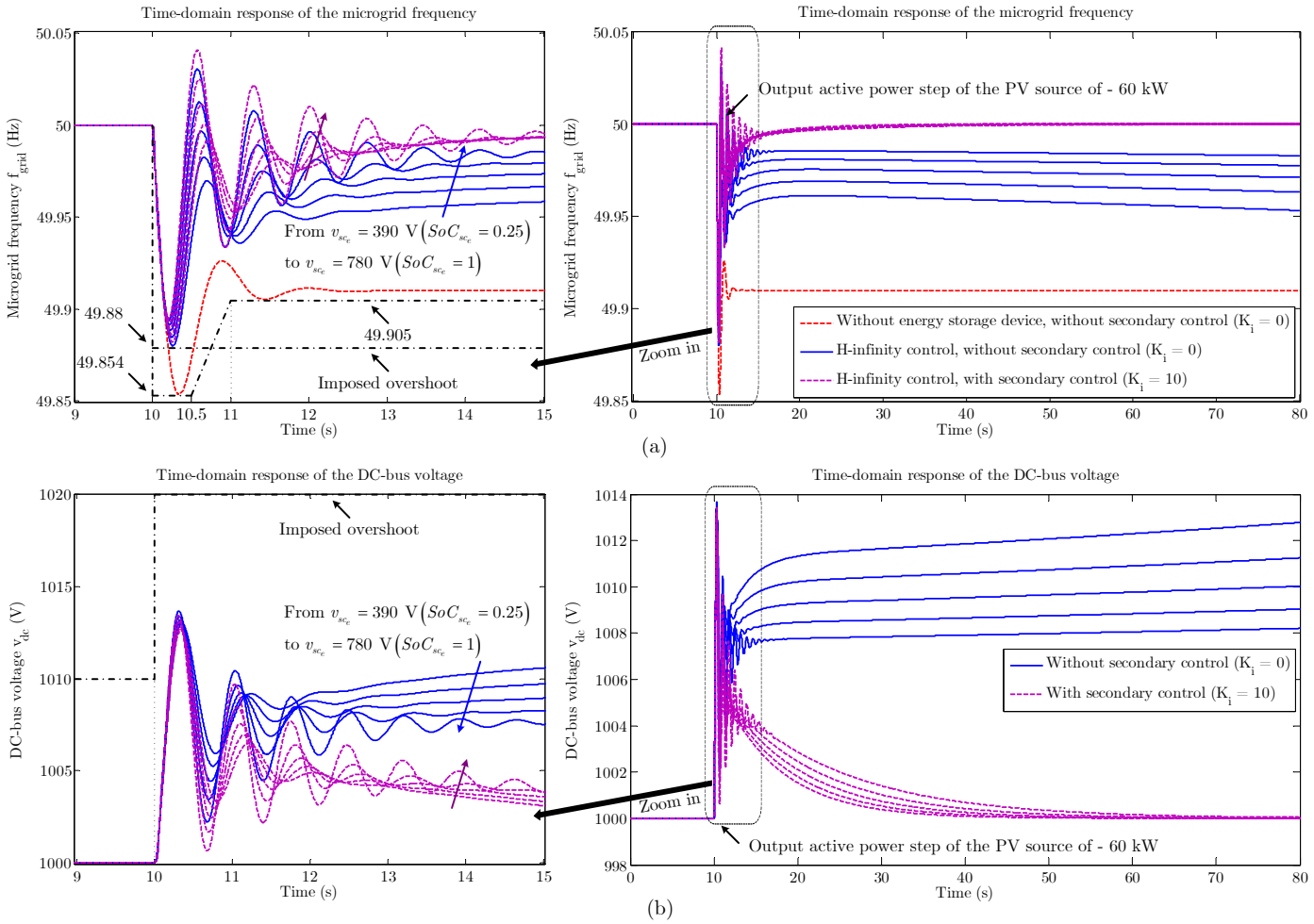

Fig. 13. (a) MG frequency time-domain responses f_{grid} and (b) DC-bus voltage time-domain responses v_{dc} under a PV output active power step disturbance of $-$ 60 kW taking into account the uncertainty in v_{sc_e} (or SoC_{sc_e}).

The sampled uncertain sensitivity functions $S(s)$, complementary sensitivity functions $KS(s)$ obtained with 33.3% uncertainty in v_{sc_e} around its design value, 585 V (i.e., $SoC_{sc_e} \in [25, 100]$ % or $v_{sc_e} \in [390, 780]$ V) and corresponding templates of the closed-loop system are presented in Fig. 12. It can be observed that, irrespective of the parametric uncertainty in v_{sc_e}, these functions are well-located below the corresponding weights, which means that the imposed overshoot performance specifications are guaranteed.

MATLAB®/Simulink® time-domain simulations using the nonlinear averaged model are carried out with a PV output active power step disturbance of $-$ 60 kW at $t = 10$ s. The supercapacitor voltage v_{sc}, in the simulation model, appears as a time-variant parameter (i.e., $\Delta v_{sc} \neq 0$). The initial value of SoC_{sc} is varied between 25% and 100% in simulation. As predicted by analyzing the sampled uncertain sensitivity functions $S(s)$, complementary sensitivity functions $KS(s)$, and corresponding templates in Fig. 12, as well as seen in Fig. 13(a) and Fig. 13(b), the closed-loop control overshoot performances of the frequency f_{grid} and the DC-bus voltage v_{dc} are preserved regardless of the initial value of SoC_{sc}. Hence, the synthesized $\mathcal{H}_\infty$ controller is robust in performance to $SoC_{sc_e} \in [25, 100]$ % (or $v_{sc_e} \in [390, 780]$ V). The time-domain responses of the energy storage device current i_s and the inverter output current in d–axis i_{rd} taking into account the uncertainty in v_{sc_e} are given in Fig. 14(a) and Fig. 14(b), respectively.

8. CONCLUSION AND FUTURE WORK

A complete time/frequency-domain analysis, including a sensitivity analysis, has been performed for frequency robust control in stand-alone MGs with PV sources. Simulation results show the effectiveness of the proposed control approach. This points out that the synthesized $\mathcal{H}_\infty$ controller remains robust in performance to the large uncertainty in the initial value of SoC_{sc} (in particular $SoC_{sc_e} \in [25, 100]$ %), which is quite good for practical operation of the supercapacitor-based energy storage system as long as the corresponding variations of the supercapacitor current are considered admissible.

Future work can concern design of a robust control strategy for PCC voltage regulation. Experimental tests for control validation on a real-time test bench are also envisaged.

9. REFERENCES

[1] N. Hatziargyriou, H. Asano, R. Iravani, and C. Marnay, "Microgrids," *IEEE Power Energy Mag.*, vol. 5, no. 4, pp. 78–94, Jul./Aug. 2007.

[2] D. E. Olivares, A. Mehrizi-Sani, A. H. Etemadi, C. A. Cañizares, R. Iravani, M. Kazerani, A. H. Hajimiragha, O. Gomis-Bellmunt, M. Saeedifard, R. Palma-Behnke, G. A. Jiménez-Estévez, and N. D. Hatziargyriou, "Trends in

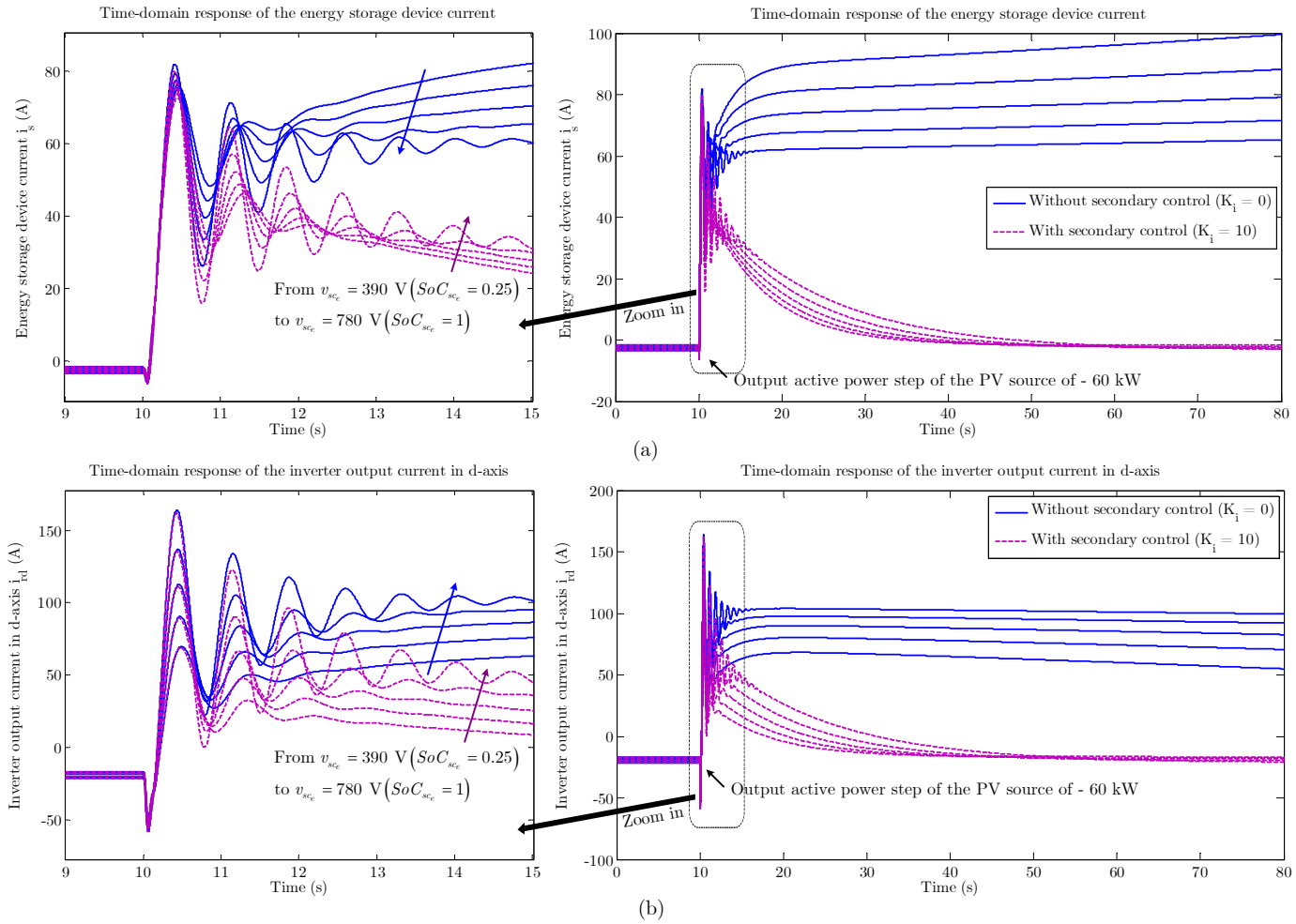

Fig. 14. (a) Time-domain responses of the energy storage device current i_s and (b) Time-domain responses of the inverter output current in d–axis i_{rd} under a PV output active power step disturbance of $-$ 60 kW taking into account the uncertainty in v_{sc_e} (or SoC_{sc_e}).

microgrid control," *IEEE Trans. Smart Grid*, vol. 5, no. 4, pp. 1905–1919, Jul. 2014.

[3] M. Chilali and P. Gahinet, "$\mathcal{H}_\infty$ design with pole placement constraints : an LMI approach," *IEEE Trans. Autom. Control*, vol. 41, no. 3, pp. 358–367, Mar. 1996.

[4] T. Goya, E. Omine, Y. Kinjyo, T. Senjyu, A. Yona, N. Urasaki, and T. Funabashi, "Frequency control in isolated island by using parallel operated battery systems applying $\mathcal{H}_\infty$ control theory based on droop characteristics," *IET Renew. Power Gener.*, vol. 5, no. 2, pp. 160–166, Mar. 2011.

[5] V. P. Singh, S. R. Mohanty, N. Kishor, and P. K. Ray, "Robust $\mathcal{H}_\infty$ load frequency control in hybrid distributed generation system," *Int. J. Elect. Power Energy Syst.*, vol. 46, pp. 294–305, Mar. 2013.

[6] A. Kahrobaeian and Y. A. R. I. Mohamed, "Direct single-loop μ–synthesis voltage control for suppression of multiple resonances in microgrids with power-factor correction capacitors," *IEEE Trans. Smart Grid*, vol. 4, no. 2, pp. 1151–1161, Jun. 2013.

[7] A. Kahrobaeian and Y. A. R. I. Mohamed, "Robust single-loop direct current control of LCL-filtered converter-based DG units in grid-connected and autonomous microgrid modes," *IEEE Trans. Power Electron.*, vol. 29, no. 10, pp. 5605–5619, Oct. 2014.

[8] M. J. Hossain, H. R. Pota, M. A. Mahmud, and M. Aldeen, "Robust control for power sharing in microgrids with low-inertia wind and PV generators," *IEEE Trans. Sustain. Energy*, vol. 6, no. 3, pp. 1067–1077, Jul. 2015.

[9] P. Li, Z. Yin, J. Zhang, and D. Xu, "Modelling robustness for a flexible grid-tied photovoltaic generation system," *IET Renew. Power Gener.*, vol. 9, no. 4, pp. 315–322, May 2015.

[10] H. Bevrani, M. R. Feizi, and S. Ataee, "Robust frequency control in an islanded microgrid : $\mathcal{H}_\infty$ and μ–synthesis approaches," *IEEE Trans. Smart Grid*, vol. 7, no. 2, pp. 706–717, Mar. 2016.

[11] Y. Han, P. M. Young, A. Jain, and D. Zimmerle, "Robust control for microgrid frequency deviation reduction with attached storage system," *IEEE Trans. Smart Grid*, vol. 6, no. 2, pp. 557–565, Mar. 2015.

[12] Q. L. Lam, A. I. Bratcu, and D. Riu, "Systematic multi-variable $\mathcal{H}_\infty$ control design for primary frequency regulation in stand-alone microgrids with high penetration of renewable energy sources," *15th Europ. Control Conf.*, Jun./Jul. 2016 (accepted for presentation).

[13] S. Skogestad and I. Postlethwaite, *Multivariable Feedback Control : Analysis and Design*. John Wiley & Sons, New York, 2005.

[14] Q. L. Lam, A. I. Bratcu, D. Riu, and J. Mongkoltanatas, "Multi-variable $\mathcal{H}_\infty$ robust control applied to primary frequency regulation in microgrids with large integration of photovoltaic energy source," in *Proc. IEEE Int. Conf. Ind. Technol.*, pp. 2921–2928, Mar. 2015.